Check for updates

An improved ASM-GDA approach to evaluate the production kinetics of loosely bound and tightly bound extracellular polymeric substances in biological phosphorus removal process†

Hai Cui,[a] Shan-Shan Yang, [iD] *[a] Ji-Wei Pang,[a] Hai-Rong Mi,[b] Chen-Chen Nuer[b] and Jie Ding[a]

This study established an extended activated sludge model no. 2 (ASM2) for providing a new recognition of the contributions of both loosely-bound EPS (LB-EPS) and tightly-bound EPS (TB-EPS) into phosphorus (P) removal by incorporating their formation and degradation processes during the anaerobic–aerobic cycle. For determining the best-fit values for the new model parameters ($k_{h,TB-EPS}$, $k_{h,LB-EPS}$, $f_{PP,TB-EPS}$, and $f_{PP,LB-EPS}$) in this extended ASM2, a novel and convenient gradient descent algorithm (GDA) based ASM (ASM-GDA) method was developed. Sensitivity analysis of $f_{PP,TB-EPS}$, $f_{PP,LB-EPS}$, $k_{h,TB-EPS}$, and $k_{h,LB-EPS}$ on the model target outputs of S_{PO_4}, X_{TB-EPS}, X_{LB-EPS}, and X_{PP} proved the accuracy of the chosen parameters. Eight batch experiments conducted under different influential chemical oxygen demand (COD) and P conditions were quantitatively and qualitatively analyzed. Respectively, 9.37–9.64% and 4.17–4.29% of P removal by TB-EPS and LB-EPS were achieved. Self-Organizing Map (SOM) has shown its high performance for visualization and abstraction for exhibiting the high correlations of the influential COD/P concentrations and the P% removal by TB-EPS (and LB-EPS). Comprehensive analyses of the influences of influential COD and P concentration on the biological phosphorus removal process help us in successfully establishing the mechanism kinetics of production and degradation of P in a dynamic P biological-treatment model.

1. Introduction

Biological phosphorus removal (BPR) plays an important role in controlling the eutrophication of a water body.[1] The success of the BPR process relies mainly on a group of selectively enriched polyphosphate accumulating organisms (PAOs) with phosphorus uptake ability.[2,3] It is conventionally considered that the accumulated P by PAOs is transformed to polyphosphate (polyP) and stored inside the cells.[4] However, recent studies reveal that microbial cells embedded in their surrounding matrix of EPS collectively form a semi-solid structure and exhibit an important role in biological waste-water treatment processes.[5–7] As a complex high-molecular-weight mixture of polymers, the accepted consensus for EPS classification in the literature contains the tightly bound EPS (TB-EPS) forming the inner layer, the loosely bound EPS (LB-EPS) diffusing in the outer layer, and soluble EPS originating

from EPS hydrolysis.[8,9] As an inevitable transportation pathway of P between bulk solution and PAOs cell, both TB-EPS and LB-EPS are regarded as the P reservoirs, and hence pose significantly influences on the uptake and release of P in BPR processes. More recently, some studies have already provided a new recognition of the contribution of both the LB-EPS and TB-EPS into P removal by proposing a new BPR metabolic model.[10] Thereby, it is of great important to learn the roles of LB-EPS, TB-EPS and microbial cells in the contribution and dynamics of P removal in the BPR processes.

Mathematical modeling has proven to be essential for understanding the reaction mechanism and kinetics of the complex biological wastewater treatment processes.[11] Established earlier by the International Water Association (IWA), popularly used activated sludge models (ASMs) have provided researchers and practitioners with a standardized set of the mechanism model for the biological treatment processes.[12–15] Although researches on ASMs mathematical models have contributed to increasing knowledge in the BPR field,[16,17] the reaction mechanism by incorporating and exploring the roles of TB-EPS and LB-EPS in BPR process in ASM models were not presented in literatures. To gain a better understanding of the

[a]State Key Laboratory of Urban Water Resource and Environment, Harbin Institute of Technology, Harbin 150000, PR China. E-mail: shanshanyang@hit.edu.cn

[b]College of Aerospace and Civil Engineering, Harbin Engineering University, Harbin 150001, PR China

role of EPS in the transformation and transportation of P in a dynamic biological-treatment model, kinetics model of the formation and hydrolysis of X_{TB-EPS} and X_{LB-EPS} being accompanied by new model parameters (new kinetic and stoichiometric parameters) are established in an improved ASM2 in this study. The quantitative determination of the contents and species of P in the formation and hydrolysis of LB-EPS and TB-EPS as well as their kinetics in BPR processes are comprehensively studied.

But what is strikingly noticeable is that, the focus on the applications of ASMs in wastewater treatment and on related research has been on the extension or improvement of traditional ASMs,[18–21] comparatively little attention has been paid to develop a convenient and applicable methodology for determining the model parameters of these Monod-based equations, even though this aspect is equally important to the models development. Traditional methods for the evaluation of kinetic parameters require representative data and linearized fitting methods to fit the nonlinear kinetic equations to the data.[22] However, there are deficiencies in the use of applying linearized fitting methods to the nonlinear kinetic equations in ASMs which have been recognized for many years, as discussed repeatedly in literatures.[22] Additionally, some available measurements for model parameters are often estimated using trial and error methods, and no parameter confidence interval is given, and no independent model validation is provided.[23] Therefore, other than the complicated chemical methods or complex models, the importance of developing an effective and convenient methodology for determining the model parameters in the new established LB-EPS and TB-EPS kinetic models is highly emphasized.

Pertaining to machine learning algorithms, a gradient descent algorithm (GDA), which can be used to tune the parameters to best fit a training set of input–output pairs, is a significant general algorithm for experiential learning.[24] A GDA is also a quick and effective method for searching extreme values *via* large, or even infinite sample spaces.[25] Possessing significant advantages over traditional methods in the domain of biological wastewater treatment, an improved GDA using the method of ASMs for determining the model coefficients can be applied to any databases and experimental/environmental conditions; meanwhile, it requires no restriction conditions (*e.g.*, temperature, reactor configuration, sewage type, weather, climate, *etc.*) while establishing the model. In this paper, we develop a novel method for determining the best-fit values for the model parameters in ASMs using an improved GDA based ASM (ASM-GDA) method. To the best of our knowledge, this novel ASM-GDA method with the effective and convenient features is for the first time developed to determine the best-fit values for the model parameters in the improved or extended ASMs in this study.

The objective of this study is to elucidate the relationship between the variations in TB-EPS, LB-EPS, and P components in the anaerobic–aerobic process. An extended ASM2 kinetic modeling by incorporating three new components of X_{TB-EPS}, X_{LB-EPS}, and S_{EPS} is established to better understand the dynamics and their important roles in the BPR process.

Another significant contribution of this work is the development of an effective and convenient ASM-GDA approach to determine the best-fit values of the new model parameters. Then experimental data are used to validate this approach. Finally, eight batch experiments conducted under different influential chemical oxygen demand (COD) and P were compared to quantitatively and qualitatively describe the kinetics of LB-EPS and TB-EPS by Self-Organizing Map (SOM) and GDA model.

2. Materials and methods

2.1. Experimental setup and operation

Two parent bench-scale sequencing batch reactors (SBRs) were used in the present work with a diameter of 15 cm, a height of 35 cm and a working volume of 5.0 L, as configured in Fig. 1. Each SBR was seeded to maintain a mixed liquor suspended solids (MLSS) of 3500 ± 500 mg L^{-1} with activated sludge from a municipal wastewater treatment plant in Harbin. Two SBRs were individually operated under 10.0 ± 0.5 °C (SBR$_{\#1}$) and 20.0 ± 0.5 °C (SBR$_{\#2}$). The constant temperature for the SBRs was maintained by a precision thermostatic bath circulator with the digital temperature controller (Ningbo Tianheng Instrument factory, Ningbo, China). Air was supplied from the bottom of the reactor by aerators and the dissolved oxygen (DO) concentration was maintained at 3.0 mg L^{-1} during aerobic phase. The DO concentration in each SBR was measured and controlled precisely by a DO probe with a DO industrial intelligent controller (SUP-DM2800, Hangzhou Sinomeasure automation Technology Co., LTd, China). Electric mechanical stirrer was performed to prevent sludge settling, which were run constantly except the time for settling, feeding and decanting. The detailed time schedules for the two SBRs were operated as follows: instantaneous filling, a 2 h of anaerobic period, 3 h of aerobic period, 40 min of sludge settling period, 15 min of decanting period, and 5 min of idling idle phase, making a complete 6 h per cycle. Each SBR was operated for 4 cycles per day. During operation, the pH was maintained at 7.50 ± 0.05 by two automatic titration units
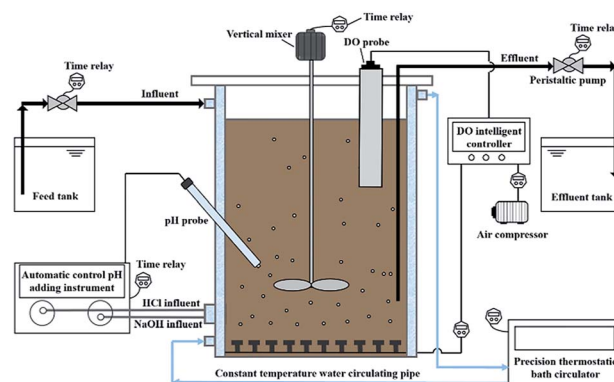

Fig. 1 Schematic representation of the lab-scale anaerobic/aerobic SBR system.

(SC-200A, ChangSha Sichen Instrument Technology Co., LTd, China) dosing 1 M HCl and NaOH to avoid the phosphate precipitation. During testing, the synthetic wastewater used as the influent of the two SBRs contained: 256.4 mg L^{-1} sodium acetate (in chemical oxygen demand), 38.2 mg L^{-1} NH$_4$Cl, 43.9 mg L^{-1} KH$_2$PO$_4$, 40 mg L^{-1} CaCl$_2$, 75 mg L^{-1} MgSO$_4$ and a trace element solution was further added as described by.[26] After about 2 months' cultivation, the sludge characteristics and effluent concentrations in the two SBRs were maintained in steady states. Each measurement was performed in triplicate.

To further quantitatively and qualitatively describe the roles of TB-EPS and LB-EPS in the BPR process, eight batch experiments conducted under different influential chemical oxygen demand (COD) concentrations varied from 150 to 300 mg L^{-1} and influential P concentrations varied from 6 to 15 mg L^{-1} were conducted: COD and P = 150 and 6 mg L^{-1} (#1); 150 and 7.5 mg L^{-1} (#2); 200 and 8 mg L^{-1} (#3); 200 and 10 mg L^{-1} (#4); 250 and 10 mg L^{-1} (#5); 250 and 12.5 mg L^{-1} (#6); 300 and 12 mg L^{-1} (#7); 300 and 15 mg L^{-1} (#8). The COD/P ratios between 20 and 25 recommended for enhanced BPR processes based on previous researches were adopted.[27,28]

2.2. Model development

2.2.1. Kinetics of formation and hydrolysis of EPS.
An extended ASM2 model for evaluating the role of the formation and degradation processes of LB-EPS, TB-EPS, and P in activated sludge and liquid phase is established in this work.

The kinetic rates expressions (ρ_i) of the extended ASM2 are shown in Table S1 (ESI).† The values of the kinetic and stoichiometric parameters together with their definitions are shown in Table S2.† The stoichiometric matrixes of the extended ASM2 are shown in Table S3.†

In this extended ASM2 model, EPS is subdivided into three major fractions: the tightly bound EPS (TB-EPS,$X_{TB\text{-}EPS}$) forming inner layer, the loosely bound EPS (LB-EPS,$X_{LB\text{-}EPS}$) diffusing in outer layer, and the soluble EPS (S_{EPS}) which is also called soluble microbial products (SMP), are weakly bound with the microbial cells or dissolved into bulk solution as the biomass-associated products (BAP).[9,29–31]

The production and degradation processes of LB-EPS using a Monod-based kinetics were described as proportional to the production of $X_{LB\text{-}EPS}$ with a stoichiometric parameter of $k_{LB\text{-}EPS}/Y_H$. The anaerobic and aerobic hydrolysis processes of LB-EPS convert it to S_{EPS} with stoichiometric parameters of $k_{h,LB\text{-}EPS}$. The third term is the storage and decomposing of X_{PP} with a stoichiometric parameter of $f_{PP,LB\text{-}EPS}$. Eqn (1) and (2) express the kinetic model description of $X_{LB\text{-}EPS}$ under anaerobic and aerobic processes:

$$\frac{dX_{LB\text{-}EPS}}{dt} = -\rho_4 + f_{PP,LB\text{-}EPS} \times \rho_8 \tag{1}$$

$$\frac{dX_{LB\text{-}EPS}}{dt} = \frac{k_{LB\text{-}EPS}}{Y_H} \times \rho_1 - \rho_4 + f_{PP,LB\text{-}EPS}(\rho_6 + \rho_8) \tag{2}$$

Similarly, eqn (3) and (4) describe the kinetic equation for the model description of $X_{TB\text{-}EPS}$ under anaerobic and aerobic processes:

$$\frac{dX_{TB\text{-}EPS}}{dt} = -\rho_3 + f_{PP,TB\text{-}EPS} \times \rho_8 \tag{3}$$

$$\frac{dX_{TB-EPS}}{dt} = \frac{k_{TB-EPS}}{Y_H}\rho_1 + \rho_3 + f_{PP,TB-EPS}(\rho_6 + \rho_8) \tag{4}$$

2.2.2. Kinetics of production and degradation of P.
In this extended ASM2 model, LB-EPS and TB-EPS acted as the P reservoirs with respective stoichiometric parameters of $f_{PP,LB\text{-}EPS}$ and $f_{PP,TB\text{-}EPS}$. Regarding the roles of LB-EPS and TB-EPS in the contribution and dynamics of P removal under alternating anaerobic/aerobic process, the aerobic storage of X_{PP} describes the degradation of S_{PO_4} with a stoichiometric parameter $1 - f_{PP,TB\text{-}EPS} - f_{PP,LB\text{-}EPS}$. Eqn (5) and (6) describe the kinetics of the production and degradation of S_{PO_4} under anaerobic and aerobic processes:

$$\frac{dS_{PO_4}}{dt} = v_{3,PO_4} \times \rho_3 + v_{4,PO_4} \times \rho_4 + Y_{PO_4} \times \rho_5 + (1 - f_{PP,TB\text{-}EPS}$$
$$- f_{PP,LB\text{-}EPS})\rho_8 + v_{10,PO_4} \times \rho_{10} + v_{11,PO_4} \times \rho_{11} \tag{5}$$

$$\frac{dS_{PO_4}}{dt} = -\left[i_{P,X_{TB\text{-}EPS}} \times \frac{k_{TB\text{-}EPS}}{Y_H} + i_{P,X_{LB\text{-}EPS}} \times \frac{k_{LB\text{-}EPS}}{Y_H} + i_{P,BM}\right.$$
$$\times (1 - k_{TB\text{-}EPS} - k_{LB\text{-}EPS})\bigg]\rho_1 + v_{2,PO_4} \times \rho_2 + v_{3,PO_4} \times \rho_3$$
$$+ v_{4,PO_4} \times \rho_4 + Y_{PO_4} \times \rho_5 - \rho_6 + (1 - f_{PP,TB\text{-}EPS} - f_{PP,LB\text{-}EPS})$$
$$\times \rho_8 - i_{P,BM} \times \rho_9 + v_{10,PO_4} \times \rho_{10} + v_{11,PO_4} \times \rho_{11} \tag{6}$$

2.3. A novel ASM-GDA method for the determination of kinetic and stoichiometric parameters coefficients

First, we suppose the size of the sample space of the influent–effluent qualities is m, the space of the kinetic coefficient is n, and that j is the sampling set, i is the components in ASMs, $X_{out}{}^i(j)$ represents the predictive effluent quality, and $Y_{out}{}^i(j)$ represents the actual effluent quality.

According to the ordered pairs of the predictive-actual effluent quality, the fitting of these n kinetic coefficients is conducted in m sample spaces. The fitting function is defined as eqn (7):

$$J(\cdot) = \sum_{j=1}^{m}\left\{\sum_{i=1}^{m}\frac{1}{2}\left[X_{out}{}^i(j) - Y_{out}{}^i(j)\right]^2\right\} \tag{7}$$

The GDA is adopted for its minimum value points (eqn (8)),

$$k_i(r+1) = k_i(r) - \alpha\frac{\partial J(\cdot)}{\partial k_i} \tag{8}$$

where k_i is the i_{th} kinetic and stoichiometric parameters. We suppose that the initial values of k_i are the typical values of the ASM

model at 20 °C, that α is the step length of the descending gradient, and that $k_i(r+1)$ and $k_i(r)$ are the recursive transfer modes.

Thus, to find the partial derivative of eqn (7) on each dynamic coefficient, eqn (9) shows:

$$
\begin{aligned}
\frac{\partial J(\cdot)}{\partial k_i} &= \sum_{j=1}^{m}\left\{\sum_{i=1}^{n}\left[X_{\text{out}}{}^i(j) - Y_{\text{out}}{}^i(j)\right] \times \frac{\partial\left[X_{\text{out}}{}^i(j) - Y_{\text{out}}{}^i(j)\right]}{\partial k_i}\right\} \\
&= \sum_{j=1}^{m}\left\{\sum_{i=1}^{n}\left[X_{\text{out}}{}^i(j) - Y_{\text{out}}{}^i(j)\right] \times \frac{\partial X_{\text{out}}{}^i(j)}{\partial k_i}\right\}
\end{aligned}
\tag{9}
$$

Also, according to the ASM model, we have (eqn (10)),

$$
\frac{\mathrm{d}X_i}{\mathrm{d}t} = f_i(X_1 \ldots X_n)
\tag{10}
$$

where X_i is the concentration of the transient value of the i_{th} component, and the function $f_i(X_1 \ldots X_n)$ is the expression of the transient value of the concentrations of the components in the ASMs. Eqn (10) can be expressed as follows:

$$
X_{\text{out}}{}^i(j) - X_{\text{in}}{}^i(j) = \int_0^T f_i(X_i \ldots X_n)\mathrm{d}t
\tag{11}
$$

where T is the reaction period corresponding to the hydraulic retention time (HRT).

Thus, eqn (11) can be expressed as follows:

$$
X_{\text{out}}{}^i(j) - X_{\text{in}}{}^i(j) = \int_0^T f_i(X_1 \ldots X_n)\mathrm{d}t = \sum_{t=1}^{h} f_1\left(X_1{}^t \ldots X_n{}^t\right)\Delta t
\tag{12}
$$

where $X_i{}^t$ is the concentration of the transient value of the i_{th} component at time t. The numerical solution of eqn (10) can be obtained via the Runge–Kutta method; $\Delta t = \dfrac{T}{h}$ is the step length of the Runge–Kutta method. Therefore,

$$
X_{\text{out}}{}^i(j) = \sum_{t=1}^{h} f_i\left(X_1{}^t \ldots X_n{}^t\right)\Delta t + X_{in}{}^i(j)
\tag{13}
$$

Thus,

$$
\begin{aligned}
\frac{\partial X_{\text{out}}{}^i(j)}{\partial k_i} &= \frac{\partial\left[\sum_{t=1}^{h} f_i\left(X_1{}^t \ldots X_n{}^t\right)\Delta t + X_{in}{}^i(j)\right]}{\partial k_i} \\
&= \frac{\partial\left[\sum_{t=1}^{h} f_i\left(X_1{}^t \ldots X_n{}^t\right)\Delta t\right]}{\partial k_i} = \sum_{t=1}^{h}\Delta t\frac{\partial f_i\left(X_1{}^t \ldots X_n{}^t\right)}{\partial k_i}
\end{aligned}
\tag{14}
$$

where,

$$
\frac{\partial f_i\left(X_1{}^t \ldots X_n{}^t\right)}{\partial k_i} = \frac{f_i(X_1 \ldots X_n, k_1 \ldots k_n)}{\partial k_i}
\tag{15}
$$

Furthermore, as can be seen from the ASM model, the function $f_i(\cdot)$ can be expressed as a function of $X_i{}^t$, as well as a function of k_i. Thus, bringing eqn (14) into eqn (9), eqn (9) can be expressed using the following equation:

$$
\begin{aligned}
\frac{\partial J(\cdot)}{\partial k_i} &= \sum_{j=1}^{m}\left\{\sum_{i=1}^{n}\left[X_{\text{out}}{}^i(j) - Y_{\text{out}}{}^i(j)\right] \times \left[\sum_{t=1}^{h}\Delta t\frac{\partial f_i\left(X_1{}^t \ldots X_n{}^t\right)}{\partial k_i}\right]\right\} \\
&= \Delta t\sum_{j=1}^{m}\left\{\sum_{i=1}^{n}\left[X_{\text{out}}{}^i(j) - Y_{\text{out}}{}^i(j)\right] \times \left[\sum_{t=1}^{h}\frac{\partial f_i\left(X_1{}^t \ldots X_n{}^t\right)}{\partial k_i}\right]\right\}
\end{aligned}
\tag{16}
$$

Additionally, bringing eqn (16) into eqn (8), eqn (8) can be expressed using the following:

$$
\begin{aligned}
k_i(r+1) = k_i(r) &- \alpha\Delta t\sum_{j=1}^{m}\left\{\sum_{i=1}^{n}\left[X_{\text{out}}{}^i(j) - Y_{\text{out}}{}^i(j)\right]\right. \\
&\left.\times\left[\sum_{t=1}^{h}\frac{\partial f_i\left(X_1{}^t \ldots X_n{}^t\right)}{\partial k_i}\right]\right\}
\end{aligned}
\tag{17}
$$

Therefore, to conduct the programming based on eqn (17), the optimal fitting kinetic coefficient n in a particular sample space is obtained through the comprehensive consideration of ASMs and the actual influent–effluent qualities of the numerically ordered pairs.

2.4. Analytical methods

2.4.1. EPS extractions and analyses. Both the LB-EPS and TB-EPS of the aerobic and anaerobic sludge samples were extracted using a modified heat extraction method.[30] Extractions of LB-EPS and TB-EPS were filtrated through 0.45 μm acetate cellulose membranes. The contents of LB-EPS and TB-EPS extractions were analysed for total organic carbon (TOC), proteins, carbohydrates, and humic-like substances, respectively.[30] COD, soluble COD (SCOD), ammonia nitrogen (NH_4^+-N), total phosphate (TP), phosphate (PO_4^{3-}-P), TP in bulk solution (TP solution), TP in LB-EPS ($TP_{\text{LB-EPS}}$), TP in TB-EPS ($TP_{\text{TB-EPS}}$), MLSS, MLVSS, and sludge volume index (SVI) were measured in accordance with the standard methods.[32] The carbohydrates was measured by anthrone-sulfuric acid method. The protein was measured with a low concentration proteins kit (Shanghai Lida Biotech CO., LTD, China). Humic substances was analyzed according to.[30] The concentration of TOC was analysed by a TOC analyzer (SHIMADZU TOC-VCPN Total Organic Carbon analyzer, USA). The polyP in activated sludge was measured according to the method in the study of.[33] Measurement of poly(β-hydroxybutyrate) (PHB) was performed as described in the study of ref. 34.

3. Results and discussion

3.1. Overall performance of two SBRs

Two lab-scale SBRs performed under 10 ± 0.5 and 20 ± 0.5 °C generally reached steady-state after 1 month inoculation. As shown in Fig. 2a, the MLVSS/MLSS ratio in the two SBRs gradually increased from 55% at the beginning of inoculation up to 92–93% at the steady state, suggesting the well enrichment of biomass during the acclimation period. Fig. 2b shows the
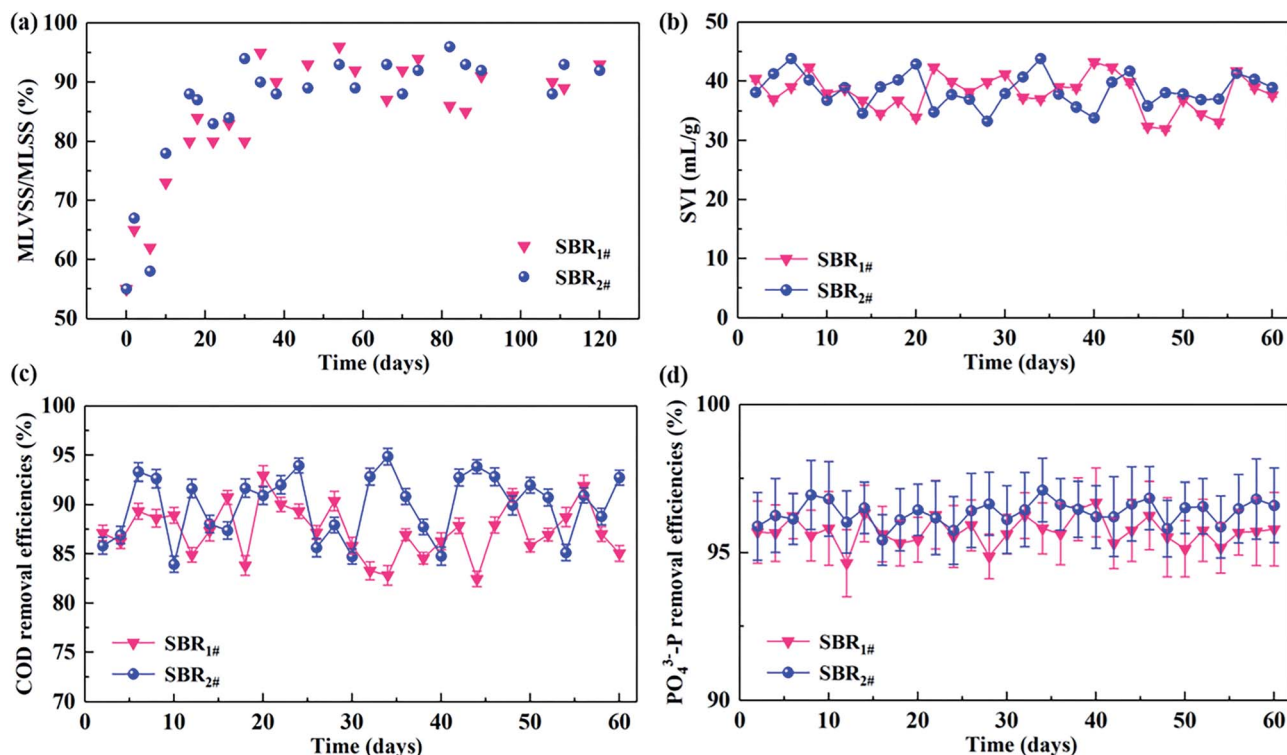
Fig. 2   Variations of (a) MLVSS/MLSS ratio, (b) SVI, (c) COD, and (d) PO_4^{3-}-P in $SBR_{\#1}$ and $SBR_{\#2}$ under 10.0 ± 0.5 and 20.0 ± 0.5 °C.

observed values of SVI in $SBR_{1\#}$ and $SBR_{2\#}$ during 60 day steady operation. It can be clearly observed that good SVI values around 31–44 mL g^{-1} in $SBR_{1\#}$ and $SBR_{2\#}$ indicated that SBRs operated under 10 °C and 20 °C had no distinguished differences in their settling abilities.

The alternating anaerobic–aerobic cycle behaviors of COD and P in the effluents of the two SBRs over 60 day steady state were given in Fig. 2c and d. By inoculating an average influent COD concentration of 200 ± 6.85 mg L^{-1}, average effluent COD concentrations in $SBR_{1\#}$ and $SBR_{2\#}$ were respective 25.19 ± 0.77 and 20.11 ± 1.01 mg L^{-1}, corresponding to the COD removal efficiencies were 87.38 ± 0.82 and 89.91 ± 0.85%, respectively (Fig. 2c). In terms of P removal, the effluent PO_4^{3-}-P concentrations in the effluent were respective 0.43 ± 0.10 and 0.37 ± 0.11 mg L^{-1} for $SBR_{1\#}$ and $SBR_{2\#}$ (Fig. 2d). By comparison, average PO_4^{3-}-P removal efficiencies of 95.71 ± 0.98 and 96.36 ± 1.09% in $SBR_{1\#}$ and $SBR_{2\#}$ were observed. Compared with $SBR_{\#1}$ operated under 10 ± 0.5 °C, better COD and P removal abilities in $SBR_{\#2}$ can be observed over 60 days operation period.

3.2.   Changes in contents of P, LB-EPS and TB-EPS of two SBRs

The profiles of the LB-EPS and TB-EPS contents in $SBR_{\#1}$ and $SBR_{\#2}$ were showed in Fig. 3a and b. After about 2 months' cultivation, activated sludge under 10 °C reaction had an initial TB-EPS and LB-EPS contents of 116.38 ± 4.91 and 16.19 ± 0.66 mg g^{-1} MLSS, while differentiated initial TB-EPS and LB-EPS contents of 130.34 ± 5.73 and 20.65 ± 0.85 mg g^{-1} MLSS were observed under 20 °C reaction period, suggesting that the

contents of LB-EPS and TB-EPS were obviously influenced by the operational temperature. For both the SBRs, the contents of TB-EPS in activated sludge were much higher than those of LB-EPS. Obvious increases in contents of TB-EPS and LB-EPS were observed during external substrate consumption. After the external substrate was completely depleted, both LB-EPS and TB-EPS concentrations did not change significantly, indicating that the formation of both the TB-EPS and LB-EPS mainly occurred during the external substrate consumption period, which this observation was in accordance with the unified theory for EPS production proposed by ref. 29.

The operational temperature was also found has significant influences on the contents of carbohydrates, proteins, and humic substances in LB-EPS and TB-EPS (Fig. 3c and d). For the contents of TB-EPS and LB-EPS formed at 10 °C (Fig. 3c), proteins were the predominant component at quantities of 42.45–48.98%, followed by carbohydrates at 32.32–38.84%, while the contents of humic substances accounted for a relative smaller proportion of the TB-EPS and LB-EPS (13.93–20.48%). The predominance of protein contents in the LB-EPS and TB-EPS might be induced by the formation of a large quantity of exoenzymes due to the easy degradation and uptake of readily biodegradable organic acetate, as suggested by previous studies.[30,35] While for $SBR_{\#2}$ as shown in Fig. 3d, the predominant content contained in TB-EPS and LB-EPS was carbohydrates. Higher carbohydrates contained in both TB-EPS and LB-EPS in $SBR_{\#2}$ by comparing those of $SBR_{\#1}$ might be induced by their different environmental and operational conditions, as well as their different microbial communities formed during 60
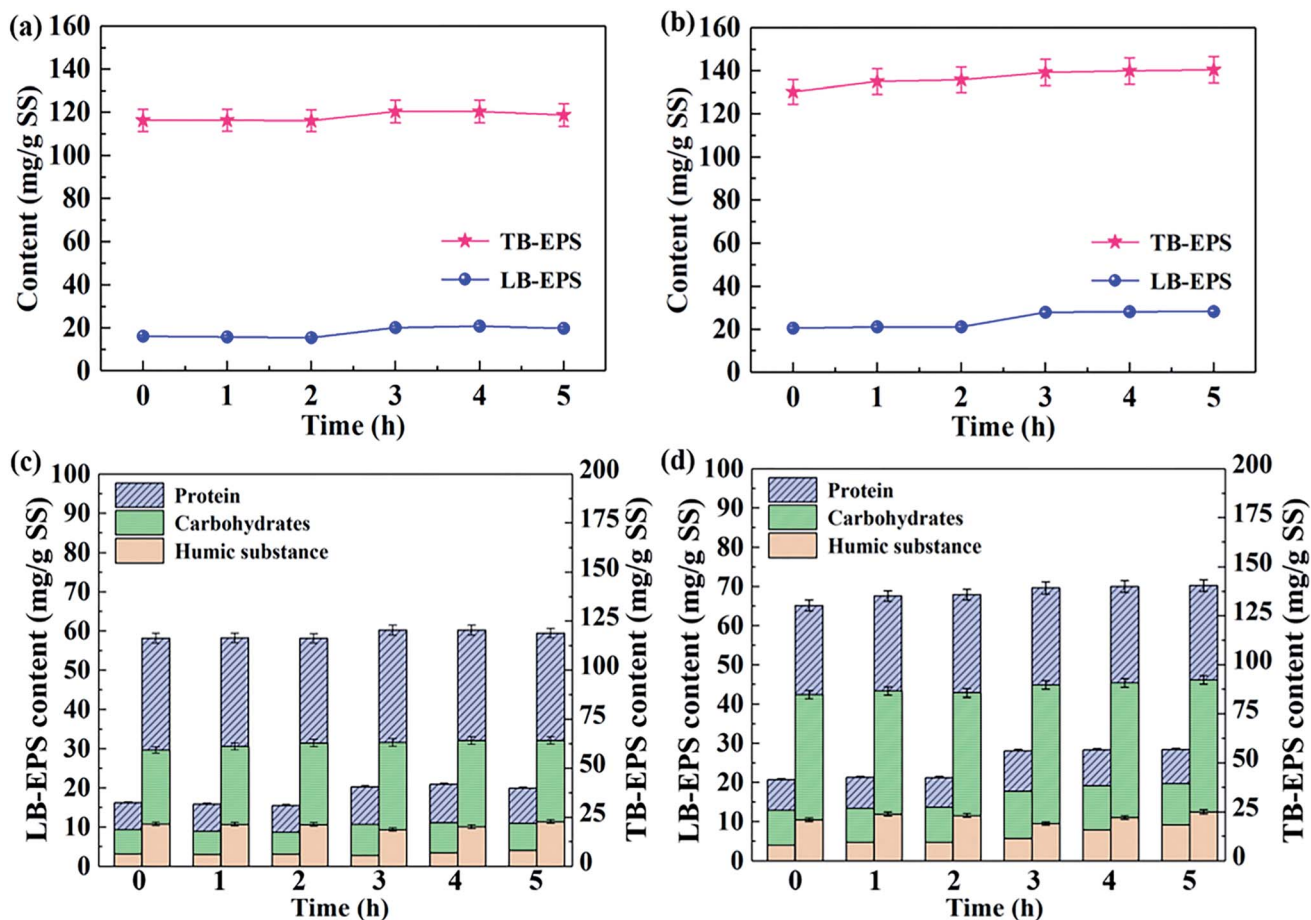
Fig. 3   Variations in (a and b) the LB-EPS and TB-EPS contents and (c and d) the carbohydrates, proteins, and humic substances contents in the TB-EPS and LB-EPS during the anaerobic–aerobic cycle under 10.0 ± 0.5 and 20.0 ± 0.5 °C.

day steady operation.[30,36] According to previous investigations,[2,37] higher carbohydrates content in EPS was found beneficial for EPS phosphorus removal. Combined with analyses of operation observation in Fig. 2, higher carbohydrates content contained in TB-EPS and LB-EPS might have helped in improving the performance of P removal in $SBR_{\#2}$. The results obtained from the analyses of the carbohydrates, proteins, and humic substances contents in LB-EPS and TB-EPS could provide a better explanation of why the effluent quality from $SBR_{\#2}$ (20 °C) systems was better than that from $SBR_{\#1}$ operated under 10 °C.

Table 1 showed the increased P contents in TB-EPS and LB-EPS from $SBR_{\#1}$ and $SBR_{\#2}$ at the end of aerobic adsorption. Operated under 20 °C in one cycle, up to 3.08 ± 0.12 mg L^{-1} and 1.37 ± 0.06 mg L^{-1} of P increased in TB-EPS and LB-EPS had been observed in $SBR_{\#2}$, which respective $9.52 \pm 0.37\%$ and $4.23 \pm 0.19\%$ of P removal by TB-EPS and LB-EPS were found after 3 h aerobic reaction. Compared with $SBR_{\#1}$, increased P contents in TB-EPS and LB-EPS were relatively lower than those from $SBR_{\#2}$ operated under 20 °C, thus might explain better performance of P removal in $SBR_{\#2}$. Results indicated that TB-EPS played a more important role than LB-EPS. To better understand the dynamics and the important roles of TB-EPS

and LB-EPS in BPR process, the data set from $SBR_{\#2}$ operated under 20 °C was chosen for investigations on the extended ASM2 development in the following section.

3.3.   Application of ASM-GDA method

The values of the kinetic and stoichiometric parameters are shown in Table S2.† New parameters of $k_{h,TB-EPS}$, $k_{h,LB-EPS}$, $f_{PP,TB-EPS}$, and $f_{PP,LB-EPS}$ to elucidate the relationship between the variations in TB-EPS, LB-EPS, and P components in the anaerobic–aerobic process are determined based on eqn (11)–(19). Fig. 4 expresses the three-dimensional display of five-dimensional spaces: 3-D plots represent the ε_{Error} convergence curves under the four new parameters by using the proposed ASM-GDA method. In this study, the data set in Fig. 3 (operated under 20 °C) is applied to estimate the kinetic parameters, then the red curves represented the gradient descent direction, are described to determine these new parameters, $k_{h,TB-EPS}$, $k_{h,LB-EPS}$, $f_{PP,TB-EPS}$, and $f_{PP,LB-EPS}$ (Fig. 4). As shown in Fig. 4, at the terminal of red curve, the extreme point, that is, the final value of the parameter can be found. The partial derivative matrixes of the four parameters derived in eqn (18) and (19) are built to get the optimal values under respective anaerobic and aerobic reactions.

Table 1 Contents of components in activated sludge from SBR$_{\#1}$ and SBR$_{\#2}$ during the anaerobic–aerobic cycle under 10.0 ± 0.5 and 20.0 ± 0.5 °C

	10 °C		20 °C	
Components	Initial[a]	Final[b]	Initial[a]	Final[b]
MLSS (mg L^{-1})	3583 ± 117	3486 ± 126	3583 ± 117	3448 ± 139
TB-EPS content (mg g^{-1} MLSS)	116.38 ± 4.91	118.91 ± 5.23	130.34 ± 5.73	140.49 ± 6.18
LB-EPS content (mg g^{-1} MLSS)	16.19 ± 0.66	19.88 ± 0.82	20.65 ± 0.85	28.40 ± 1.16
Protein in TB-EPS (mg g^{-1} MLSS)	57.00 ± 2.51	54.53 ± 2.40	45.51 ± 2.00	48.22 ± 2.12
Protein in LB-EPS (mg g^{-1} MLSS)	6.87 ± 0.28	8.92 ± 0.37	7.79 ± 0.32	8.78 ± 0.36
Carbohydrates in TB-EPS (mg g^{-1} MLSS)	37.61 ± 1.66	41.42 ± 1.82	63.76 ± 2.81	67.18 ± 2.96
Carbohydrates in LB-EPS (mg g^{-1} MLSS)	6.10 ± 0.25	6.89 ± 0.28	8.85 ± 0.36	10.46 ± 0.43
Humic substances in TB-EPS (mg g^{-1} MLSS)	21.76 ± 0.96	22.93 ± 1.01	21.06 ± 0.93	25.09 ± 1.10
Humic substances in LB-EPS (mg g^{-1} MLSS)	3.22 ± 0.13	4.07 ± 0.17	4.01 ± 0.16	9.16 ± 0.38
Increased P content in TB-EPS (mg L^{-1})	—	2.67 ± 0.09	—	3.08 ± 0.12
Increased P content in LB-EPS (mg L^{-1})	—	0.98 ± 0.03	—	1.37 ± 0.06
Increased P content in TB-EPS (%)	—	8.64 ± 0.28	—	9.52 ± 0.37
Increased P content in LB-EPS (%)	—	3.17 ± 0.10	—	4.23 ± 0.19

[a] Represents the contents of components in activated sludge from SBR#1 and SBR#2 at the beginning of anaerobic reaction. [b] Represents the contents of components in activated sludge from SBR#1 and SBR#2 at the end of aerobic reaction.

$$\frac{\partial \left(\frac{\mathrm{d}X_i}{\mathrm{d}t}\right)}{\partial k_j} = \begin{bmatrix} \dfrac{0.02 x_2 x_7}{0.02 + x_2} & \dfrac{0.02 x_2 x_8}{0.02 + x_2} & \dfrac{-0.2 x_5 x_{13}}{0.02 + x_5} & \dfrac{-0.2 x_5 x_{13}}{0.02 + x_5} \\ \dfrac{x_2 x_7}{0.02 = x_2} & \dfrac{x_2 x_8}{0.02 = x_2} & & \\ -\dfrac{x_2 x_7}{0.02 = x_2} & & \dfrac{0.2 x_5 x_{13}}{0.1 = x_5} & \\ & -\dfrac{x_2 x_8}{0.02 + x_2} & & \dfrac{0.2 x_5 x_{13}}{0.1 + x_5} \end{bmatrix} + \begin{bmatrix} 0 \\ 0 \\ 0 \\ 1 \end{bmatrix} \frac{1.5 x_1 x_3 x_5 x_{12} x_{14}(0.34 x_{12} - x_{13})}{(0.2 = x_1)(0.01 = x_3)(0.1 = x_5)(0.01 x_{12} + x_{14})(0.36 x_{12} - x_{13})}$$

(18)

$$\frac{\partial \left(\frac{\mathrm{d}X_i}{\mathrm{d}t}\right)}{\partial k_j} = \begin{bmatrix} \dfrac{0.02 x_2 x_7}{0.02 + x_2} & \dfrac{0.02 x_2 x_8}{0.02 + x_2} & \dfrac{-0.2 x_5 x_{13}}{0.02 + x_5} & \dfrac{-0.2 x_5 x_{13}}{0.02 + x_5} \\ \dfrac{x_2 x_7}{0.02 + x_2} & \dfrac{x_2 x_8}{0.02 + x_2} & 0 & 0 \\ -\dfrac{x_2 x_7}{0.02 + x_2} & 0 & \dfrac{0.2 x_5 x_{13}}{0.1 + x_5} & 0 \\ 0 & -\dfrac{x_2 x_8}{0.02 = x_2} & 0 & \dfrac{0.2 x_5 x_{13}}{0.1 + x_5} \end{bmatrix}$$

(19)

where x_1, x_2, x_3, x_5, x_6, x_7, x_8, x_{12}, x_{13}, and x_{14} represent S_O, S_S, S_{PO_4}, S_{ALK}, S_{EPS}, $X_{TB\text{-}EPS}$, $X_{LB\text{-}EPS}$, X_{PAO}, X_{PP}, and X_{PHA} in the extended ASM2 model (Table S3†). j represents $k_{h,TB\text{-}EPS}$, $k_{h,LB\text{-}EPS}$, $f_{PP,TB\text{-}EPS}$, and $f_{PP,LB\text{-}EPS}$, respectively. To computing the partial derivatives of the four new parameters, the anaerobic and aerobic matrixes of 4×4 are obtained in eqn (18) and (19). The error convergence curve (ε_{Error}) and α are set as 10^{-4} and 0.1, respectively.

Based on the derived partial derivative matrixes, the three-dimensional display of the five-dimensional space, including ε_{Error}, $k_{h,TB\text{-}EPS}$, $k_{h,LB\text{-}EPS}$, $f_{PP,TB\text{-}EPS}$, and $f_{PP,LB\text{-}EPS}$, is depicted in

Fig. 4. In our work, one experiment was conducted to estimate the initial values. After 50 156 iterations by the proposed ASM-GDA, the $k_{h,TB\text{-}EPS}$, $k_{h,LB\text{-}EPS}$, $f_{PP,TB\text{-}EPS}$, and $f_{PP,LB\text{-}EPS}$, values were calculated as 0.228 d^{-1}, 0.4 d^{-1}, 0.09 S_{PO_4} per g$X_{TB\text{-}EPS}$, and 0.04 S_{PO_4} per g$X_{LB\text{-}EPS}$, respectively. To evaluate the extent to whether the new parameters used in the extended ASM2 can influence the target output variables (S_{PO_4}, $X_{TB\text{-}EPS}$, $X_{LB\text{-}EPS}$, and X_{PP}), the coefficients $\delta_{i,j}$ of the four new parameters are calculated (eqn (S1)†). According to the sensitivity analysis in ESI,† a 50% increase in the input variable is applied for calculating the normalised sensitivity coefficient ($\delta_{i,j}$) in this study. Fig. 5 displays the sensitivity analysis of $f_{PP,TB\text{-}EPS}$, $f_{PP,LB\text{-}EPS}$, $k_{h,TB\text{-}EPS}$, and $k_{h,LB\text{-}EPS}$ on the model outputs of S_{PO_4}, $X_{TB\text{-}EPS}$, $X_{LB\text{-}EPS}$, and X_{PP}. The sequence of the four parameters influencing the effluent PO$_4^{3-}$-P concentrations was $f_{PP,TB\text{-}EPS} < k_{h,LB\text{-}EPS} < f_{PP,LB\text{-}EPS} < k_{h,TB\text{-}EPS}$. Overall, as for the four target output variables, the coefficient $\delta_{i,j}$ for all the parameters were below 0.5, indicating that the chosen parameters have no significant influences on the four model output variables.

For this proposed novel ASM-GDA approach, few or even one data set was needed to obtain the accurate model parameters, as
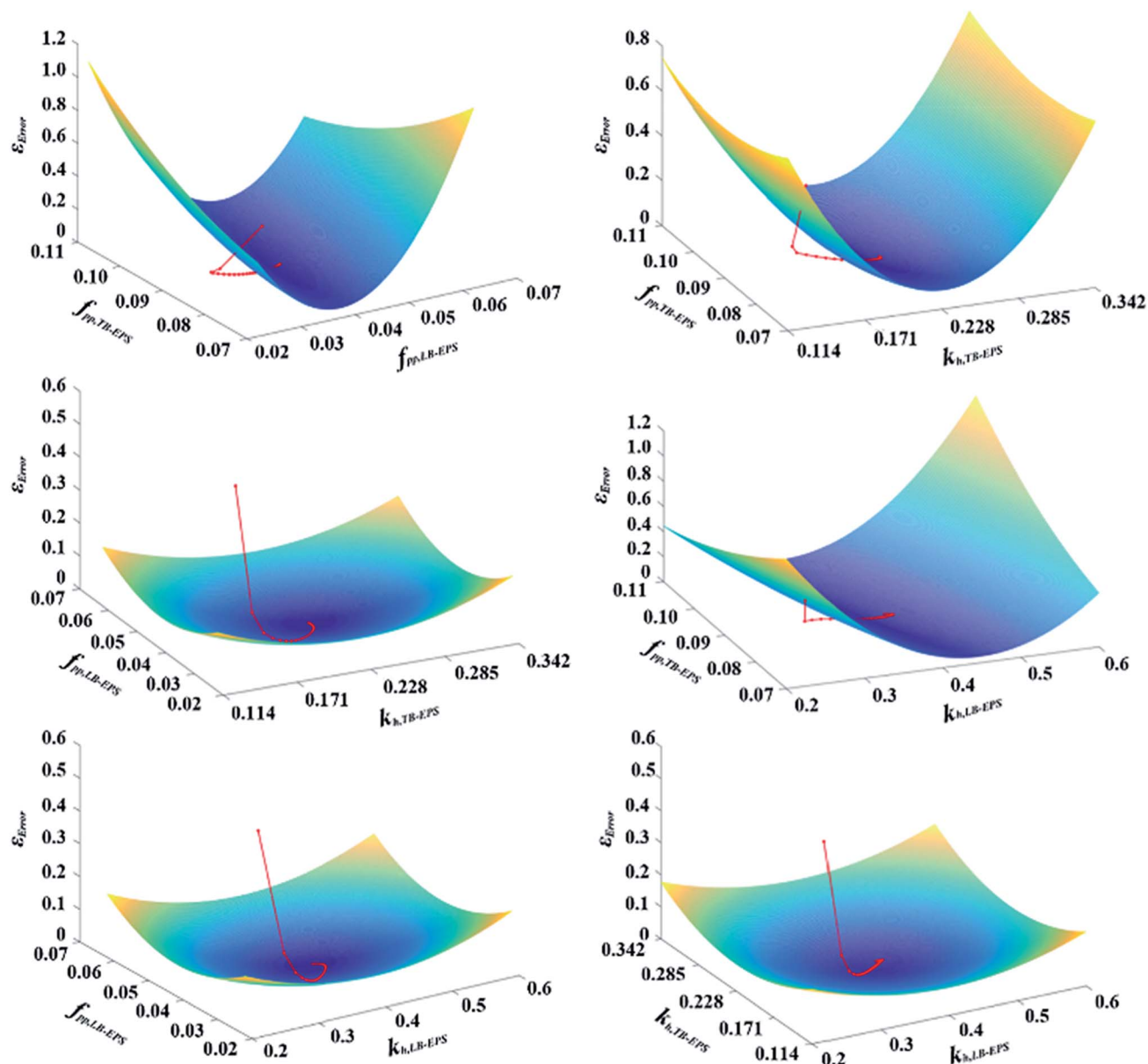
Fig. 4 Three-dimensional display of five-dimensional spaces: 3-D plots represent the ε_{Error} convergence curves under the four new parameters ($k_{h,TB-EPS}$, $k_{h,LB-EPS}$, $f_{PP,TB-EPS}$, and $f_{PP,LB-EPS}$) by using the proposed ASM-GDA method.

demonstrated in this work. Results indicated that the proposed ASM-GDA model provided a rapid, accurate, and convenient method to determine the model parameters by using any databases. The convenience and accuracy of this method are very attractive for biological wastewater treatment processes, which are typically characterized by their complexity, low repeatability, time-consumption, and the variation of uncertainty in their practical applications.

3.4. Model verification

To further evaluate the role of the formation and degradation processes of LB-EPS, TB-EPS, and P in activated sludge and liquid, model verification is conducted through comparing the

measured results and the simulated data from batch experiments conducted under different substrate concentrations. Fig. 6a and b compare the variations of the extended ASM2 model simulations and the experimental results of S_{PO_4}, X_{PP}, X_{TB-EPS}, and X_{LB-EPS}, with an influential COD of 250 mg L^{-1} and P of 10 mg L^{-1}. Being accompanied by the release and uptake processes of S_{PO_4} during the alternating anaerobic/aerobic reaction (Fig. 6a), the concentrations of X_{PP} in activated sludge changed first decreased at anaerobic process and then an upward trend at the subsequent aerobic process, while became slightly fluctuation when S_{PO_4} was completely consumed. As shown in Fig. 6a, high correlation analyses values ($R^2 = 0.987$ for S_{PO_4} and $R^2 = 0.977$ for X_{PP}) of measured results and simulated data indicated that the model outputs from the
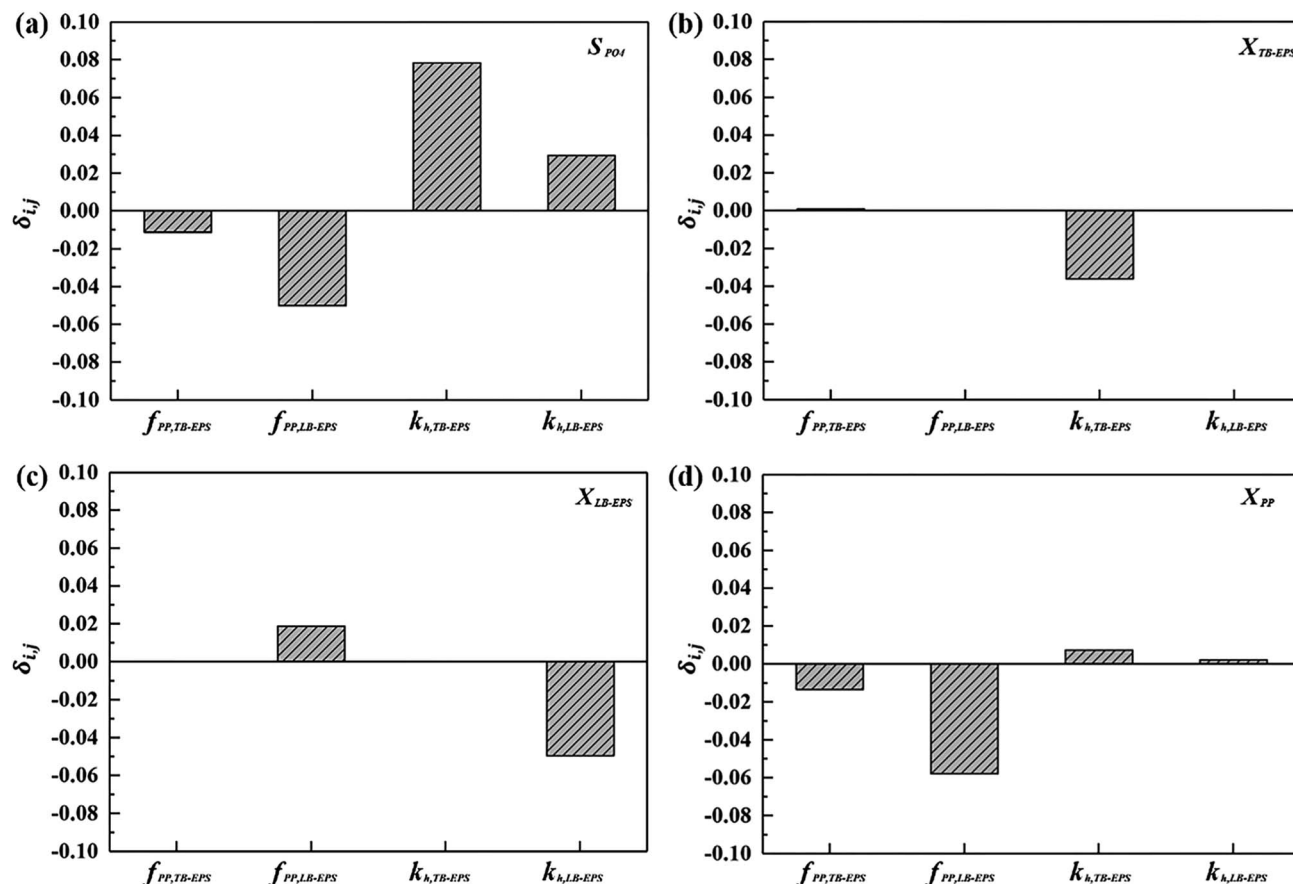
Fig. 5 Sensitivity analysis of $f_{PP,TB-EPS}$, $f_{PP,LB-EPS}$, $k_{h,TB-EPS}$, and $k_{h,LB-EPS}$ on the model outputs: (a) S_{PO_4}, (b) X_{TB-EPS}, (c) X_{LB-EPS}, and (d) X_{PP}.

extended ASM2 captured the experimental trends for this experiment in terms of the production and degradation of P under anaerobic/aerobic processes.

Observed in Fig. 6b, new components of X_{TB-EPS} and X_{LB-EPS} introduced in this extended ASM2 showed a good agreement between the model outputs and the experimental data. Compared with the simulation data, the maximum differences observed in the measured values of TB-EPS and LB-EPS was 6%, and 95% of the results had a difference of less than 5%, proving the validity of the extended ASM2 with the estimated kinetic parameters. As shown in Fig. 6b, the production of TB-EPS and LB-EPS occurred during substrate consumption period, once the substrate was completely consumed, no further increases in TB-EPS and LB-EPS contents were observed in the modelling and experimental results. Under anaerobic and the latter aerobic processes after the depletion of the external substrate, the slow downward trends in TB-EPS and LB-EPS in activated sludge were attributed to the hydrolysis of EPS or microbial decay.

To evaluate the roles of LB-EPS and TB-EPS in P removal in BPR process, the variations of P components in polyP, TB-EPS, LB-EPS were further calculated. Although 81.15% of P in the liquid was removed through the aerobic storage process of X_{PP} during aerobic reaction, respective 9.49% and 4.22% of P removal by X_{TB-EPS} and X_{LB-EPS} can be observed at the end of P aerobic absorption process. The results further confirmed that

TB-EPS played a more important role in P removal than LB-EPS. The contributions of both the TB-EPS and LB-EPS pose significantly influences on the dynamics of anaerobic P-release/ aerobic P-uptake in BPR process.

3.5. Influence of influential COD and P on the roles of TB-EPS and LB-EPS in BPR

It is noticed that the process of BPR under alternating anaerobic and aerobic process was dependent upon the initial COD and P concentrations in previous studies.[38–40] In order to better understanding the roles of TB-EPS and LB-EPS in the transformation and transportation of P in a dynamic biological-treatment model, eight batch experiments (numbered as #1, #2, ..., #8) conducted under different influential COD concentrations varied from 150 to 300 mg L^{-1} and influential P concentrations varied from 6 to 15 mg L^{-1} were tested. To analyse the correlation between the influential COD/P concentrations and the P% removal by TB-EPS (and LB-EPS) at the end of aerobic stage, a Self-Organizing Map (SOM), an unsupervised artificial neural network learning algorithm, is applied and details are described in ESI.† Fig. 6c displays the component planes of the intrinsic relationships of the four input data sets obtained from the eight batch experiments. Clustering by SOM, each input data set can be mapped into 25 output neurons being represented by hexagon in the subgraph (Fig. 6c). SOM can extract the eigenvalues of the
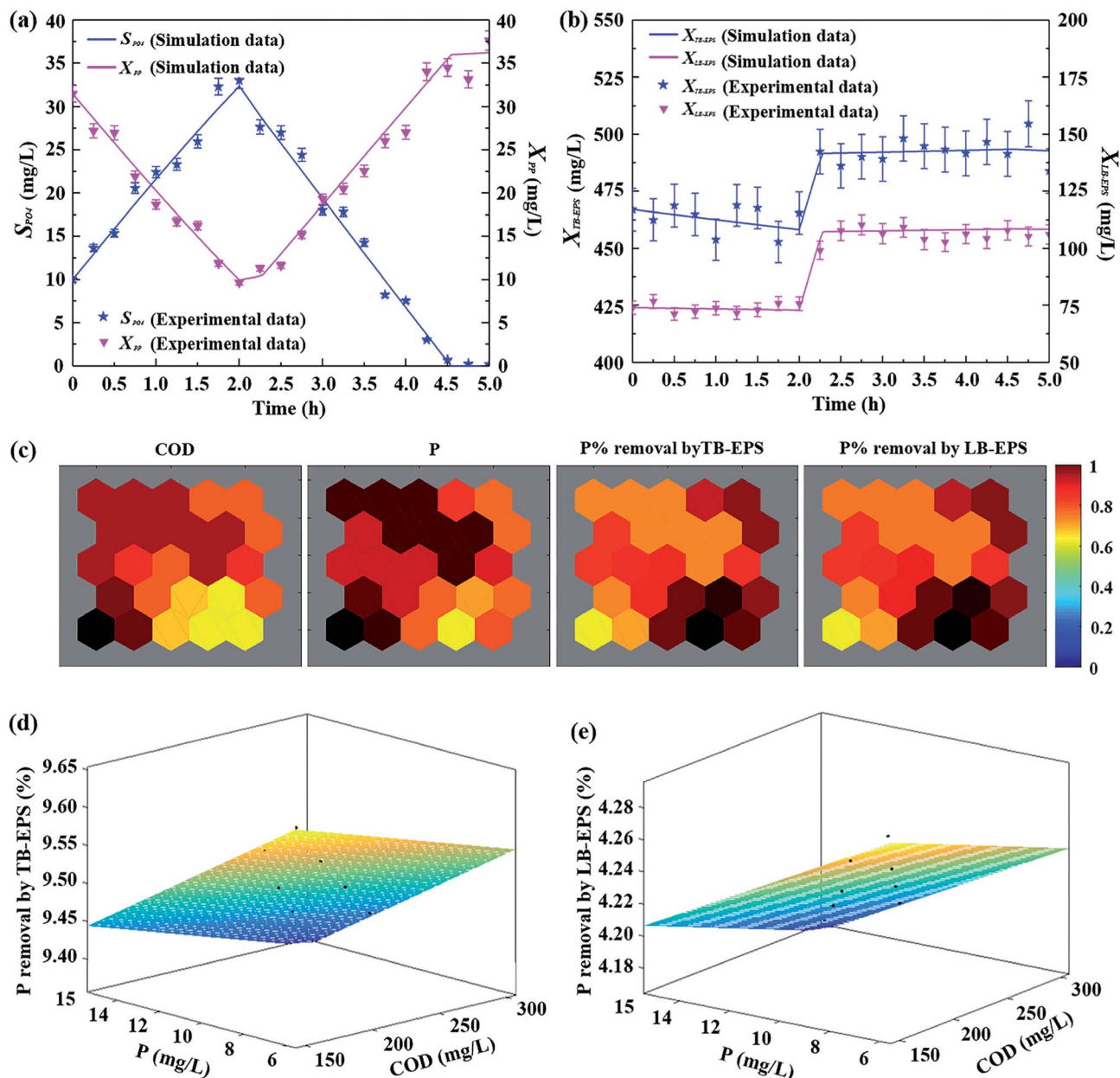
Fig. 6 The experimental data and the extended ASM2 model simulations of (a) S_{PO_4} and X_{PP}, (b) X_{TB-EPS} and X_{LB-EPS}; (c) abstract visualization of the relationships between influential COD concentration, influential P concentration, P% removal by TB-EPS, and P% removal by LB-EPS using an SOM model; (d) influence analyses of the effects of initial COD and P concentrations on P removal by respective (e) TB-EPS and (f) LB-EPS using the GDA model.

original input data. The extracted eigenvalues are the output neurons in the SOM.[41] In this study, 25 output neurons are used as the feature matrix of the original data, that is, each hexagon in the graph represents a neuron in the output layer, while the number of neurons does not affect the result analysis. The weight of each eigenvalue (neuron) is represented by color.[41] Darker color represents higher correlation between each input parameter and the corresponding output neurons. Closer colors of the same intermediate parameters in different subgraphs suggest the stronger correlation between the two inputs. It can be seen from Fig. 6c, there were significantly high correlations between the 4 inputs data sets and the 25 output neurons ($r > 0.65$). Besides,

closer colors (value of chromatism < 0.2) of the corresponding output neurons sites between the influential COD (and P) and the P% removal by TB-EPS (and LB-EPS) demonstrated their stronger correlation, indicating that the SOM has shown its high performance for visualization and abstraction for exhibiting the high correlations of the influential COD/P concentrations and the P% removal by TB-EPS (and LB-EPS) during the BPR process.

Further quantitatively analyses of the effects of initial COD and P concentrations on P removal by respective TB-EPS and LB-EPS are showed in Fig. 6d and e. By inoculating with different initial COD and P concentrations, 9.37–9.64% of P removal by TB-EPS (Fig. 6d) and 4.17–4.29% of P removal by LB-EPS

(Fig. 6e) were achieved. Through the GDA model, two linear models to explain the relationship between the influential COD and P concentrations with P removal by LB-EPS and TB-EPS at the end of aerobic reaction were obtained: P% removal by TB-EPS = 9.839 − 0.0005795P − 0.02023COD; P% removal by LB-EPS = 4.276 − 0.0002833P − 0.0008372COD. A better understanding of the influence of influential COD and P on BPR processes helps us establishing a comprehensive reference for the mechanism of biological P removal by incorporating the roles of TB-EPS and LB-EPS in BPR process.

4. Conclusions

Experimental data operated under 10 °C and 20 °C were compared to discuss the roles of TB-EPS and LB-EPS in the transformation and transportation of P under an anaerobic–aerobic process. Operational temperature was proved imposes significant influence on the contents of carbohydrates, proteins, and humic substances in LB-EPS and TB-EPS, as well as the capability of P removal in a BPR process.

An extended ASM2 kinetic modeling by introducing three new components of X_{TB-EPS}, X_{LB-EPS}, and S_{EPS} was established. An effective and convenient ASM-GDA approach was developed to determine the best-fit values of the new model parameters. Sensitivity analyses indicated that the influencing sequence of the four new parameters for the effluent S_{PO_4} was $f_{PP,TB-EPS} < k_{h,LB-EPS} < f_{PP,LB-EPS} < k_{h,TB-EPS}$. The model simulations matched the experimental measurements and provided a new recognition into the dynamics reaction mechanism of P by incorporating the roles of LB-EPS and TB-EPS in BPR process.

Eight batch experiments conducted under different influential COD and P were quantitatively and qualitatively analyzed. SOM has shown its high performance for visualization and abstraction for exhibiting the high correlations of the influential COD/P concentrations and the P% removal by TB-EPS (and LB-EPS) during BPR process. Through the GDA model, two linear models were obtained: P% removal by TB-EPS = 9.839 − 0.0005795P − 0.02023COD; P% removal by LB-EPS = 4.276 − 0.0002833P − 0.0008372COD. Results demonstrated that there are 9.37–9.64% of P was removed by TB-EPS and 4.17–4.29% of P was removed by LB-EPS under different influential COD concentrations varied from 150 to 300 mg L^{-1} and influential P concentrations varied from 6 to 15 mg L^{-1}.

Conflicts of interest

There are no conflicts to declare.

Acknowledgements

References

1 Y. X. Zhao, C. F. Chao, S. Y. Zhai, Z. J. Wang and M. Ji, Treatment of Rural Wastewater Using a Spiral Fiber Based Salinity-Persistent Sequencing Batch Biofilm Reactor, *Water*, 2017, **9**, 970.

2 N. Li, N. Ren, X. Wang and H. Kang, Effect of temperature on intracellular phosphorus absorption and extra-cellular phosphorus removal in EBPR process, *Bioresour. Technol.*, 2010, **101**, 6265–6268.

3 J. W. Pang, S. S. Yang, L. He, Y. D. Chen, G. L. Cao, L. Zhao, X. Y. Wang and N. Q. Ren, An influent responsive control strategy with machine learning: Q-learning based optimization method for a biological phosphorus removal system, *Chemosphere*, 2019, **234**, 893–901.

4 W. W. Li, H. L. Zhang, G. P. Sheng and H. Q. Yu, Roles of extracellular polymeric substances in enhanced biological phosphorus removal process, *Water Res.*, 2015, **86**, 85–95.

5 Q. Li, P. F. Xia, Z. Y. Tao and S. G. Wang, Modeling Biofilms in Water Systems with New Variables: A Review, *Water*, 2017, **9**, 462.

6 W. J. Zhang, B. D. Cao, D. S. Wang, T. Ma and D. H. Yu, Variations in distribution and composition of extracellular polymeric substances (EPS) of biological sludge under potassium ferrate conditioning: Effects of pH and ferrate dosage, *Biochem. Eng. J.*, 2016, **106**, 37–47.

7 B. Wang, X. Liu, J. Chen, D. Peng and F. He, Composition and functional group characterization of extracellular polymeric substances (EPS) in activated sludge: the impacts of polymerization degree of proteinaceous substrates, *Water Res.*, 2018, **129**, 133–142.

8 P. N. Hong, R. Honda, M. Noguchi and T. Ito, Optimum selection of extraction methods of extracellular polymeric substances in activated sludge for effective extraction of the target components, *Biochem. Eng. J.*, 2017, **127**, 136–146.

9 Y. Shi, J. Huang, G. Zeng, Y. Gu, Y. Chen, Y. Hu, B. Tang, J. Zhou, L. Yang and L. Shi, Exploiting extracellular polymeric substances (EPS) controlling strategies for performance enhancement of biological wastewater treatments: An overview, *Chemosphere*, 2017, **180**, 396–411.

10 X. Long, R. Tan, Z. Fang, C. Xie, Y. Li and G. Xian, The roles of loosely-bound and tightly-bound extracellular polymer substances in enhanced biological phosphorus removal, *Chemosphere*, 2017, **189**, 679–688.

11 Q. He, Q. Song, S. Zhang, W. Zhang and H. Wang, Simultaneous nitrification, denitrification and phosphorus removal in an aerobic granular sequencing batch reactor with mixed carbon sources: reactor performance, extracellular polymeric substances and microbial successions, *Chem. Eng. J.*, 2018, **331**, 841–849.

12 M. Henze, W. Gujer, T. Mino, T. Matsuo, M. C. Wentzel, G. V. R. Marais and L. M. C. M. Van, Activated sludge model No. 2d, *Water Sci. Technol.*, 1999, **39**, 165–182.

13 X. Wu, Y. Yang, G. Wu, J. Mao and T. Zhou, Simulation and optimization of a coking wastewater biological treatment process by activated sludge models (ASM), *J. Environ. Manage.*, 2016, **165**, 235–242.

14 S. Yang, W. Guo, Y. Chen, S. Peng, J. Du, H. Zheng, X. Feng and N. Ren, Simultaneous in situ sludge reduction and nutrient removal in an A2MO-M system: Performances, mechanisms, and modeling with an extended ASM2d model, *Water Res.*, 2016, **88**, 524–537.

15 J. E. Baeten, L. M. C. M. Van and E. I. P. Volcke, Modelling aerobic granular sludge reactors through apparent half-saturation coefficients, *Water Res.*, 2018, **146**, 134–145.

16 M. F. R. Zuthi, W. S. Guo, H. H. Ngo, L. D. Nghiem and F. I. Hai, Enhanced biological phosphorus removal and its modeling for the activated sludge and membrane bioreactor processes, *Bioresour. Technol.*, 2013, **139**, 363–374.

17 A. B. Lanham, A. Oehmen, A. M. Saunders, G. Carvalho, P. H. Nielsen and M. A. M. Reis, Metabolic modelling of full-scale enhanced biological phosphorus removal sludge, *Water Res.*, 2014, **66**, 283–295.

18 Z. Y. Zhu, R. Y. Wang and Y. M. Li, Evaluation of the control strategy for aeration energy reduction in a nutrient removing wastewater treatment plant based on the coupling of ASM1 to an aeration model, *Biochem. Eng. J.*, 2017, **124**, 44–53.

19 B. Ni, R. Zeng, F. Fang, W. Xie, G. Sheng and H. Yu, Fractionating soluble microbial products in the activated sludge process, *Water Res.*, 2010, **44**, 2292–2302.

20 J. Climent, L. Basiero, R. Martínez-Cuenca, J. G. Berlanga, B. Julián-López and S. Chiva, Biological reactor retrofitting using CFD-ASM modelling, *Chem. Eng. J.*, 2018, **348**, 1–14.

21 R. Chris, G. Sara, H. Claire, P. Julio and L. M. C. M. Van, Incorporating the influent cellulose fraction in activated sludge modelling, *Water Res.*, 2018, **144**, 104–111.

22 L. H. Smith, P. L. McCarty and P. K. Kitanidis, Spreadsheet Method for Evaluation of Biochemical Reaction Rate Coefficients and Their Uncertainties by Weighted Nonlinear Least-Squares Analysis of the Integrated Monod Equation, *Appl. Environ. Microbiol.*, 1998, **64**, 2044–2050.

23 B. Ni, F. Fang, W. Xie, J. Xu and H. Yu, Formation of Distinct Soluble Microbial Products by Activated Sludge: Kinetic Analysis and Quantitative Determination, *Environ. Sci. Technol.*, 2012, **46**, 1667–1674.

24 S. Pathan, K. G. Prabhu and P. C. Siddalingaswamy, Techniques and algorithms for computer aided diagnosis of pigmented skin lesions-A review, *Biomed. Signal Process. Control*, 2018, **39**, 237–262.

25 T. M. Mitchell, *Machine Learning*, McGraw-Hill Science/Engineering/Math, 1997, March 1, pp. 367–379, ISBN: 0070428077.

26 H. Zhang, W. Fang, Y. Wang, G. Sheng, R. Zeng, W. Li and H. Yu, Phosphorus Removal in an Enhanced Biological Phosphorus Removal Process: Roles of Extracellular Polymeric Substances, *Environ. Sci. Technol.*, 2013, **47**, 11482–11489.

27 A. Z. Gu, A. Saunders, J. B. Neethling, H. D. Stensel and L. L. Blackall, Functionally relevant microorganisms to enhanced biological phosphorus removal performance at full-scale wastewater treatment plants in the United States, *Water Environ. Res.*, 2008, **80**, 688–698.

28 A. Onnis-Hayden, N. Majed, A. Schramm and A. Z. Gu, Process optimization by decoupled control of key microbial populations: Distribution of activity and abundance of polyphosphate-accumulating organisms and nitrifying populations in a full-scale IFAS-EBPR plant, *Water Res.*, 2011, **45**, 3845–3854.

29 C. S. Laspidou and B. E. Rittmann, Non-steady state modeling of extracellular polymeric substances, soluble microbial products, and active and inert biomass, *Water Res.*, 2002, **36**, 1983–1992.

30 X. Li and S. Yang, Influence of loosely bound extracellular polymeric substances (EPS) on the flocculation, sedimentation and dewaterability of activated sludge, *Water Res.*, 2007, **41**, 1022–1030.

31 G. Yu, P. He and L. Shao, Characteristics of extracellular polymeric substances (EPS) fractions from excess sludges and their effects on bioflocculability, *Bioresour. Technol.*, 2009, **100**, 3193–3198.

32 *Standard Methods for the Examination of Water and Wastewater*, American Public Health Association (APHA), Washington DC, USA, 21st edn, 2005.

33 Y. Ge, *Phosphorus Removal Effect and Microbial Community Structure Analyses in the EBPR system*, Doctor's degree dissertation, Tianjin University, 2012.

34 J. Myung, W. M. Galega, J. D. Van Nostrand, T. Yuan, J. Zhou and C. S. Criddle, Long-term cultivation of a stable Methylocystis-dominated methanotrophic enrichment enabling tailored production of poly(3-hydroxybutyrate-co-3-hydroxyvalerate), *Bioresour. Technol.*, 2015, **198**, 811–818.

35 D. T. Spona, Investigation of extracellular polymer substances (EPS) and physicochemical properties of different activated sludge flocs under steady-state conditions, *Enzyme Microb. Technol.*, 2003, **32**, 375–385.

36 D. T. Sponza, Investigation of extracellular polymer substances (EPS) and physicochemical properties of different activated sludge flocs under steady-state conditions, *Enzyme Microb. Technol.*, 2003, **32**, 375–385.

37 Y. Liu, S. Yu, G. Xue and F. Zhao, Role of extracellular exopolymers in biological phosphorus removal, *Water Sci. Technol.*, 2006, **54**, 257–265.

38 Y. Wang, Y. Peng and T. Stephenson, Effect of influent nutrient ratios and hydraulic retention time (HRT) on simultaneous phosphorus and nitrogen removal in a two-sludge sequencing batch reactor process, *Bioresour. Technol.*, 2009, **100**, 3506–3512.

39 G. Bertanza, R. Pedrazzani, L. Manili and L. Menoni, Bio-P release in the final clarifiers of a large WWTP with co-precipitation: Key factors and troubleshooting, *Chem. Eng. J.*, 2013, **230**, 195–201.

40 H. Chen, Y. Liu, B. Ni, Q. Wang, D. Wang, C. Zhang, X. Li and G. Zeng, Full-scale evaluation of aerobic/extended-idle regime inducing biological phosphorus removal and its integration with intermittent sand filter to treat domestic sewage discharged from highway rest area, *Biochem. Eng. J.*, 2016, **113**, 114–122.

41 S. O. Haykin, *Neural Networks and Learning Machines*, McMaster University, Ontario Canada, 3rd edn, 2009.